

## Article

# Seabed Acoustic Mapping Revealing an Uncharted Habitat of Circular Depressions Along the Southeast Brazilian Outer Shelf

Ana Carolina Lavagnino <sup>1,\*</sup>, Marcos Daniel Leite <sup>2</sup>, Tarcila Franco <sup>1</sup> , Pedro Smith Menandro <sup>3</sup>,  
Fernanda Vedoato Vieira <sup>1</sup>, Geandré Carlos Boni <sup>1</sup>  and Alex Cardoso Bastos <sup>1,\*</sup>

<sup>1</sup> Marine Geosciences Laboratory/LaboGeo, Programa de Pós-Graduação em Oceanografia Ambiental, Departamento de Oceanografia e Ecologia, Universidade Federal do Espírito Santo, Vitória 29075910, ES, Brazil; tarcila.af@gmail.com (T.F.); fernanda.v.vieira@edu.ufes.br (F.V.V.); gcarlosboni@gmail.com (G.C.B.)

<sup>2</sup> Center of Coastal and Ocean Mapping Joint Hydrographic Center/CCOM, University of New Hampshire, Durham, NH 03824, USA; mdleite@ccom.unh.edu

<sup>3</sup> Seascapes Ecology and Mapping Lab, Department of Oceanography, Dalhousie University, Halifax, NS B3H 4R2, Canada; pedro.menandro@dal.ca

\* Correspondence: anacarolinavagnino@gmail.com (A.C.L.); alex.bastos@ufes.br (A.C.B.)

**Abstract:** Initiatives such as the United Nations Decade of Ocean Science for Sustainable Development and Seabed 2030 promote seabed mapping worldwide. In Brazil, especially on the Espírito Santo Continental Shelf, high-resolution seabed mapping has revealed an unknown complex seascape. Circular depressions (CDs) were mapped for the first time in the Costa das Algas Marine Protection Area. Herein, we aim to present the CD metrics characteristics and discuss their relationship with morphology and relevance as a habitat based on multibeam bathymetry and ground truthing. A total of 3660 depressions were mapped between 46 and 85 m in depth, reaching an area of 460 m<sup>2</sup> and 5 m relief. The continental shelf morphology was subdivided into three sectors based on morphology: inter-valleys, valley edges, and valley flanks, and eleven sites were selected for direct sampling/imaging at the CDs along the sectors. The direct sampling was carried out by scuba-diving with video images and sediment samples collected inside and outside the depressions. The deeper central parts of the circular depressions appear to function as a sink, presenting aggregations of rhodoliths or other carbonate fragments. In most inter-valley depressions, mounds were observed along the edges of the depression. We did not have any indication of gas seeps and no clear sedimentological or morphological control on their occurrence. We first hypothesize that their origin results from combined diachronous processes. The circular depressions mapped at high resolution could be related to sea level processes acting during the last glacial period and shelf exposure, i.e., relict features. The CDs are responsible for biomass aggregation and fish bioturbation, forming holes and rubble mounds, representing a modern process occurring on a centimetric scale. The data collected so far indicate that this fine-scale feature is an important habitat for different fish species. The modern maintenance of these structures could be due to low sedimentation regime areas shaped by biotic excavation.

**Keywords:** seabed habitat mapping; seafloor circular depression; high-resolution acoustic data



Academic Editor: Fabrizio Antonioli

Received: 19 November 2024

Revised: 22 December 2024

Accepted: 30 December 2024

Published: 1 January 2025

**Citation:** Lavagnino, A.C.; Leite, M.D.; Franco, T.; Menandro, P.S.; Vieira, F.V.; Boni, G.C.; Bastos, A.C. Seabed Acoustic Mapping Revealing an Uncharted Habitat of Circular Depressions Along the Southeast Brazilian Outer Shelf. *Geosciences* **2025**, *15*, 7. <https://doi.org/10.3390/geosciences15010007>

**Copyright:** © 2025 by the authors. Licensee MDPI, Basel, Switzerland.

This article is an open access article distributed under the terms and conditions of the Creative Commons Attribution (CC BY) license (<https://creativecommons.org/licenses/by/4.0/>).

## 1. Introduction

High-resolution seafloor mapping is an important tool for marine geoscience [1,2]. It allows for a wide range of thematic studies at multiple scales and motivates research related

to different terrain attributes and their suitability for habitat mapping applications [3–5]. In this context, it is common to find examples in the scientific literature involving broad-scale geodiversity analysis [6,7], monitoring seafloor changes [8,9], and fine-scale analysis of the seabed [10,11], including small features such as pits [12]. This investigation is part of mapping efforts carried out along the Espírito Santo Continental Shelf (southeast Brazil) since 2019 (Figure 1). The study site is located on the outer shelf of the Espírito Santo Continental Shelf, southeast Brazil (Figure 1). The area is part of the Costa das Algas Marine Protection Area and Santa Cruz Wildlife Refuge conservation unit, established in 2010 by a federal decree due to the high diversity of seafloor morphology and the presence of crustose coralline algae forming rhodolith beds. It is important to mention that this MPA was created without any continuous seafloor mapping (i.e., swath acoustic systems) since it is not a requirement in Brazil. Additionally, this area is only 40 km south of the Doce River mouth, an area impacted by a major environmental disaster caused by a tailing dam failure that released around 40 million m<sup>3</sup> of iron ore tailings in November 2015. The mud tailings traveled more than 600 km and reached the Doce River's mouth, creating a tailing plume that dispersed along the coast [13]. About 10 years later, environmental consequences are still observed in the area, including the MPA sediment and biota [14].

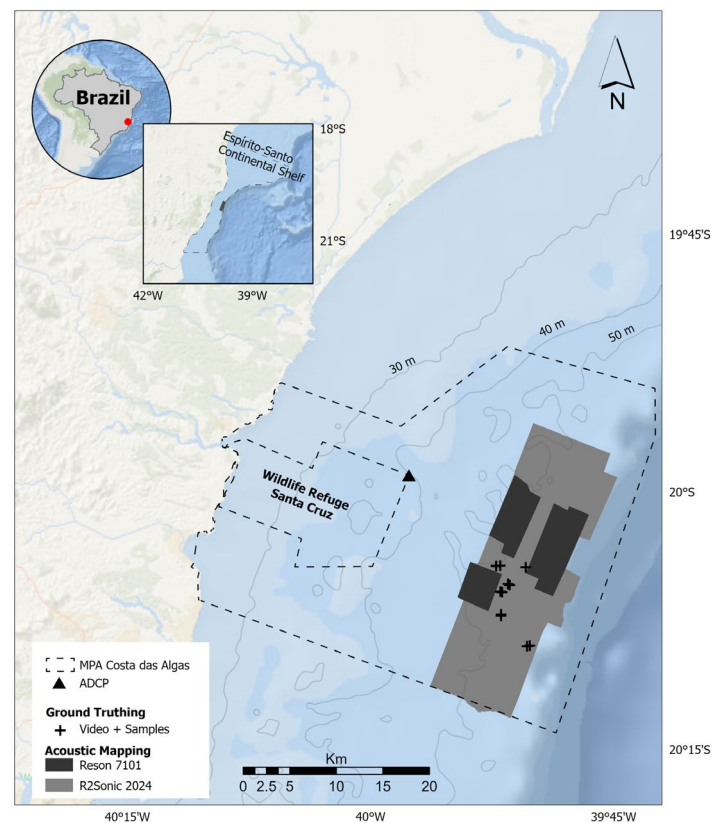


**Figure 1.** The acoustic mapping and direct sampling location in the study area in southeast Brazil, in the Espírito Santo continental outer shelf. ADCP mooring location is also shown.

Seabed relict morphology, combined with Holocene carbonate sedimentation and low sediment input, creates a complex geodiversity in the area. The surveyed region is morphologically characterized by shelf-incised valleys/paleovalleys with a heterogeneous seabed composed of rhodoliths, carbonate sediments, and low terrigenous input [15,16]. Regionally, it is well-studied in terms of the sedimentary regime and morphology [15–18] and its relation to sea-level changes [19,20]. The area is characterized by a system of shelf-incised valleys forming an important mesophotic habitat [16] and extensive rhodolith beds with varying spatial coverage [21,22]. An outreach result from this mapping program is

the detailed maps that were produced in high resolution (20 m), supporting the ongoing MPA management carried out by the Chico Mendes Institute for Biodiversity Conservation (ICMBio—Ministry of the Environment and Climate Change) [23]. By increasing the resolution even more (2 m), new smaller features were revealed—the CDs.

This high-resolution mapping program uncovered seabed features with great ecological importance, e.g., reefs [24], sand ridges close to the Doce River’s mouth [25], rhodolith beds, and shelf-incised valleys in the Costa das Algas MPA [16,21,22]. In this study, we describe for the first time fine-scale circular depressions that occur in their thousands on the shelf. Seabed circular or non-circular depressions have been mapped and described throughout continental margins worldwide, and their origin can be the result of distinct processes or substrate composition, such as gas seep-related pockmarks [26], carbonate dissolution and collapse processes, causing sinkholes [27], pit holes (biotic excavation or bioturbation) [28,29], freshwater submarine springs [30], and sediment gravity flow [31].

This study aims to investigate the CDs, in particular by (i) applying a semi-automated mapping method to map the distribution of these depressions, (ii) analyzing ground truth data collected in dedicated areas to obtain qualitative visual and sedimentological characteristics of these features, and (iii) discussing the potential origins or formation mechanisms for these depressions, with a particular focus on their potential ecological relevance as a macrohabitat.

## 2. Materials and Methods

### 2.1. Seabed Acoustic Mapping

The acoustic surveys covered a total of 230 km<sup>2</sup> from 43 to 300 m water depth using two multibeam echosounders (Figure 1). In 2018, a Reson 7101/240 kHz (inertial system: DMS 05 and DGPS) and in 2019, an R2 Sonic 2024/170 kHz (inertial system: Applanix POS MV WaveMaster INS) were deployed. Before the surveys, a patch test was carried out to calibrate for angular offset. For both campaigns, water column sound velocity, salinity, and temperature profiles were collected using a Mini Valeport SVP in 3 h intervals to apply SVP correction in post-processing and correct backscatter parameters. Data were collected using PDS for Reson and Qinsy for R2 Sonic. Elevation data were collected to provide tidal correction using an Acoustic Doppler Current Profiler (ADCP) moored close to the area (UTM 24S 7790168.58N 399721.2044E). Both bathymetry datasets were processed using Caris Hips and Sips (9.1 and 11.1) following (1) patch test values applied, (2) SVP correction applied, (3) tide correction, and (4) manual outlier cleaning. Backscatter recorded by the Reson system was processed in Caris Hips and Sips (9.1), and the dataset acquired with R2 Sonic was processed in FMGT (Fledermaus Geocoder Toolbox 7.9.6). The analysis of multi-source backscatter mosaics, collected with different systems, software, and acquisition configurations, was addressed and harmonized through the bulk shift method [32] using the R2 Sonic dataset as a reference. The final bathymetric surface (Figure 2A) and backscatter mosaic were exported at 2 m resolution (Figure 2F).

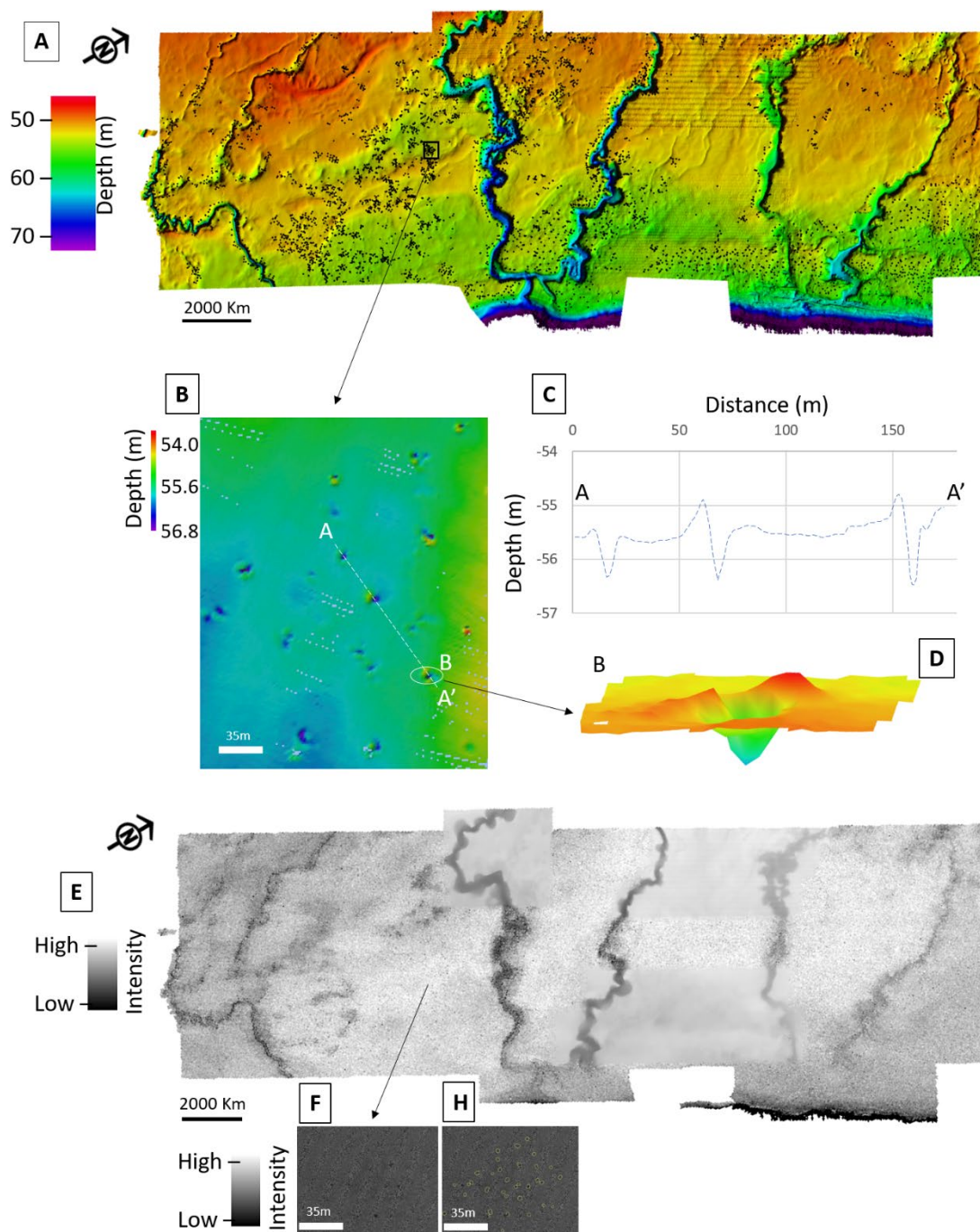


**Figure 2.** (A) Bathymetry map overlapped by circular depressions in black; (B) zoomed in is the black rectangle that depicts an area with the depressions, note that on the edges of the depression are higher reliefs; (C) a profile through 3 depressions showing the edge of the features being a positive relief; (D) a 3D view of one of the circular depressions showing aggregation of material on the sides; (E) harmonized backscatter map 20 m resolution; (F,H) a 2 m resolution backscatter insert not interpreted and interpreted as circular depressions, respectively. Note that scale inserts only account for the data within the rectangle.

## 2.2. Circular Depression Mapping

CD mapping was carried out separately on the two bathymetric datasets (not the backscatter), adopting a semi-automated method (a procedure similar to [33,34]) on the R2Sonic dataset, and using a manual delineation approach on the Reson grid due to its artifacts hindering the automated method. The delineations were compared and merged to create a final map (Figure 2). To identify circular depressions in R2Sonic, a Bathymetric

Position Index (BPI) layer (3 cells inner radius, 6 cells outer radius) was used to separate the CDs from the surrounding topography, and the resulting rasters were converted to irregular polygons (Figure 3). Polygons larger than 1000 m<sup>2</sup> and smaller than 50 m<sup>2</sup> were deleted. Polygons smaller than 50 m<sup>2</sup> can lead to incorrect identification due to data noise or by introducing outliers into the statistical analysis. Adjustment procedures were employed using ArcGIS-available tools to make irregular polygons better match circular depression edges [33]. These steps included compensating for initial delineation, which increases the polygons' area ("Buffer", "Merged", and "Dissolve") and then simplifying and smoothing the polygons ("Simplify" and "Smooth Polygon"). Statistical information for each circular depression was obtained by extracting the depth, backscatter, and slope. Values extraction was carried out by combining the GIS tools (1) "Extract by mask", which extracts the cells of a raster that corresponds to areas defined by mask and the CD polygons originating in the previous steps; (2) "Raster to point", which converts the raster dataset to point features creating an output feature class; and (3) "Spatial Join", which joins attributes from all the designated feature classes based on the spatial relationship writing then all to the output feature classes. Visual assessment was also carried out in the results to edit polygons that were incorrectly delineated. The final characterization and morphometric results calculated the following [33]: Minimum Water Depth (MinWD), Maximum Water Depth (MaxWD), Mean Water Depth (MeanWD), Relief, Area, and Perimeter. A density kernel analysis was performed on the CDs using the Spatial Analyst ArcGIS tool Kernel Density, which calculates a magnitude-per-unit area from point features.

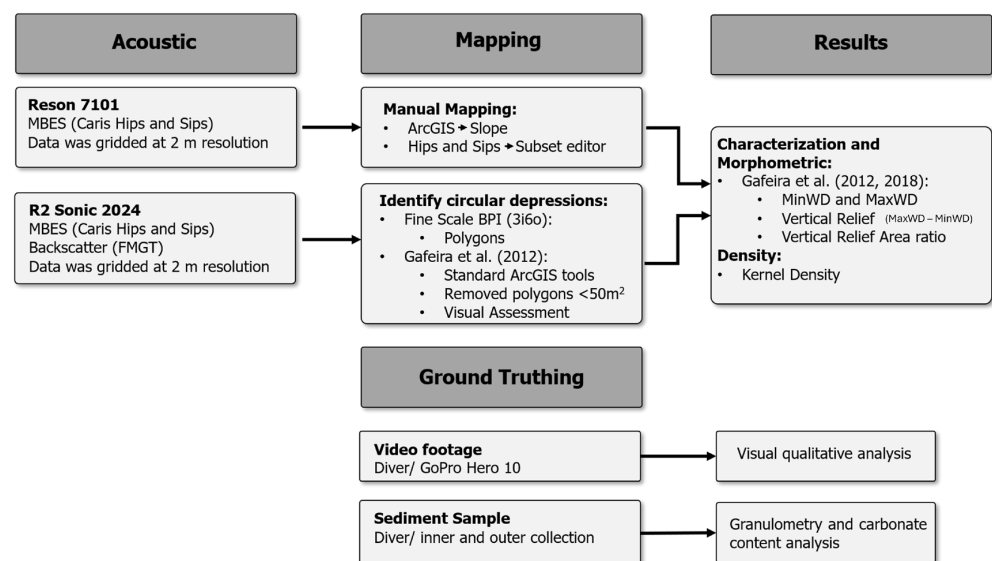


**Figure 3.** Workflow of the data processing methodology following [33,34], identification of the circular depression, and ground truthing.

### 2.3. Ground Truthing

A total of 11 diving spots (Figure 1) were located in strategic areas to obtain representative information on the sedimentology of the CDs, and 22 samples were taken from the inner and outer parts of the depressions. Diving spots were designated in areas with high concentrations of CDs. To be targeted, the depressions had to have a relatively high relief and diameter to facilitate their location by the divers (Figures 2 and 4). The samples and videos were collected in neighbor pairs, except for CD 6 (see following Figure 5 for visualization): CDs 01 and 02; CDs 08 and 10; CDs 13 and 14; CDs 15 and 16; CDs 19 and 20. The seafloor was surveyed by divers using a GoPro Hero 10 (GoPro Inc., Sao Mateo, CA, USA) camera, recording the entire depression area and arbitrarily choosing an inner and

outer point to collect sediment samples. Gravel and sand fractions were wet-sieved, and the mud fraction was analyzed using laser granulometry with a Malvern Mastersizer (2000) (Malvern Panalytical Ltd., Malvern, Worcestershire England). Grain size analyses were performed at 1 phi intervals. Carbonate content was determined by CaCO<sub>3</sub> dissolution in 30% HCl. According to [35], the samples were classified as carbonate sediments (>75% carbonate content) or mixed sediments (30–75% carbonate content).

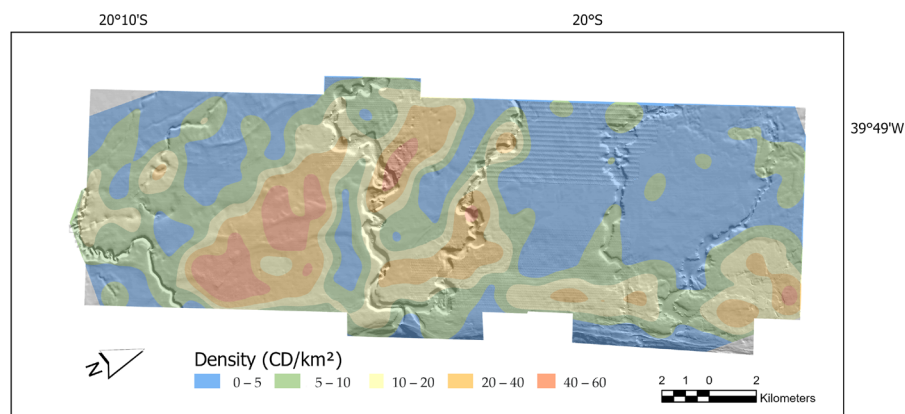


**Figure 4.** Density kernel of all mapped features (CD/km<sup>2</sup>).

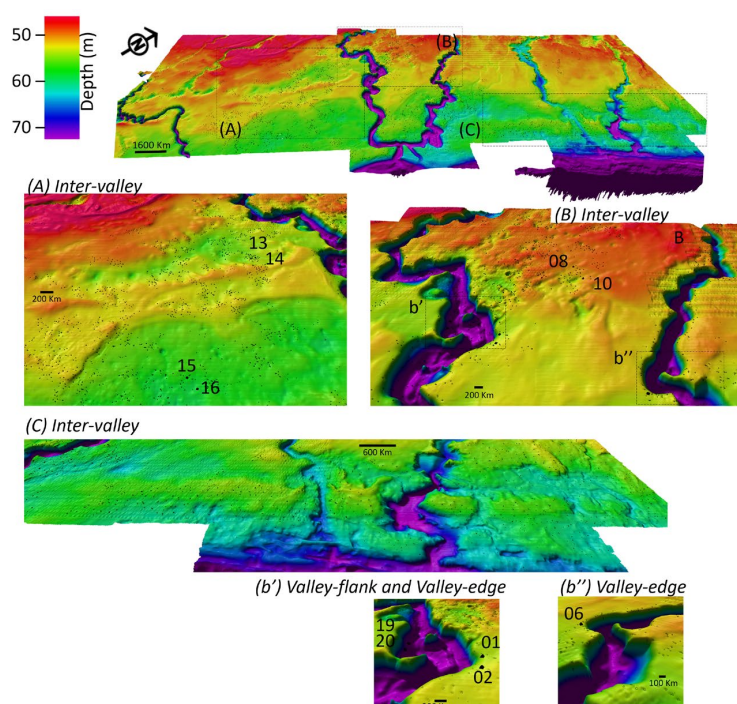


**Figure 5.** A 3D visualization of the bathymetry overlapped by the circular depressions in black; (A) inter-valley area where 4 depressions were investigated (13, 14, 15, and 16); (B) inter-valley where 2 depressions were investigated (08 and 10); (b') valley flank on the west side of the image showing depressions 19 and 20 and valley edge depressions on the east side of the image 01 and 02; (b'') valley edge depression 06; (C) region where none of the depressions were directly investigated.

### 3. Results

#### 3.1. Acoustic Mapping, Distribution, and Morphometric Characteristics

A total of 3660 CDs were mapped in this study. The semi-automatic BPI approach resulted in 2648 features, while the manual approach resulted in 1012 features. Some CDs showed positive relief on the edge-edge without indicating preferential shape or direction

(Figure 2C,D). The backscatter mosaic data for the entire area did not reveal a discernible pattern for the CDs (Figure 2E,F,H). While they frequently exhibited a lower backscatter than the adjacent region, many were indistinguishable from the adjacent seafloor.

Density kernel analysis along the area (CD per square kilometer) showed higher density values in the vicinity of the shelf valleys from the center part of the study area toward the southeast—from 20 up to 60 depressions/km<sup>2</sup>. In the northeast part of the area, density decreases, showing less than 20 depressions/km<sup>2</sup> (Figure 4).

The CDs distributed along the shelf showed great variation in area (131.86 ± 70.8 m<sup>2</sup>) and perimeter (40.68 ± 12.91 m). The relief ranged from centimeters to meters, averaging 83 cm (±0.71). Table 1 summarizes the metrics for all mapped CDs.

**Table 1.** Summary of the metrics for all the mapped circular depressions (n = 3660).

	Area (m <sup>2</sup> )	Perimeter (m)	Diameter (m)	Relief (m)
Min	25.56	18.10	5.77	−0.01
Max	459.57	114.22	36.37	−5.21
Mean	131.86	40.68	12.96	−0.83
Std Dev	70.80	12.91	4.11	0.71

The distribution of area and relief values for each CD is shown in a stacked histogram (Figure 6). The data show that the most frequent values are between 125 and 175 m<sup>2</sup> for area and between 0.5 and 0.75 m relief. The structures occupy a depth range from 46 to 85 m below sea level (Figure 2), and the stacked histogram shows that most of them are located between 50 and 60 m (Figure 6).

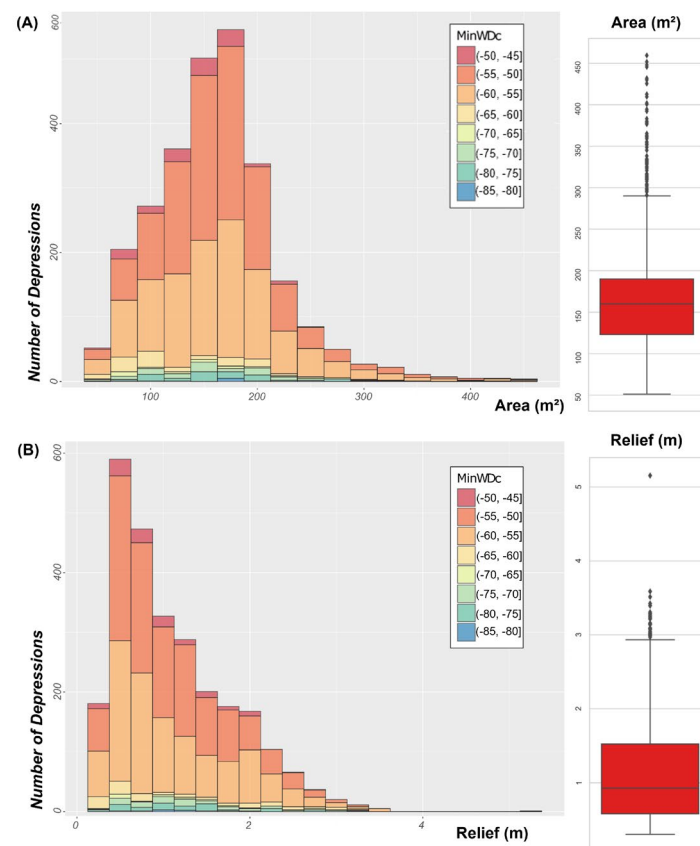


**Figure 6.** Stacked histogram showing the distribution of the circular depressions (n = 3660) depth range according to (A) area of the CD and (B) relief of the CD. Note that diamond symbol represents outliers’ measurements.

### 3.2. Circular Depression Sampling and Characterization

The CDs are distributed along the mapped area, occupying distinct morphological aspects imprinted by the shelf valleys and the flat area between the valleys (inter-valleys; Figures 2, 4, and 5). The CDs are mainly distributed within three distinct morphologies: valley edges (CD01, 02, and 06), inter-valleys (CD08, 10, 13, 14, 15), and valley flanks (CD19 and CD20) (Figure 5).

A synthesis of the interpretation of the acoustic response combined with the findings from bottom images and sediment sampling is presented for the 11 sampled CDs (Tables 2–5, Figure 7).

**Table 2.** Summary of the metrics for each surveyed circular depression.

	Area (m <sup>2</sup> )	Diameter (m)	Relief (m)	Depth (m)	Backscatter Inner—avg.		Backscatter Outside—avg (dB)
					min.	max (dB)	
CD 01	225.72	17.94	−2.15	55	−22.22	(−26.54; −18.04)	−22.30
CD 02	166.31	14.87	−2.11	54	−22.85	(−24.97; −19.93)	−22.41
CD 06	266.95	19.43	−2.55	53.5	−21.55	(−24.97; −18.67)	−20.97
CD 08	197.26	16.16	−3.14	51	−21.56	(−24.34; −18.98)	−21.42
CD 10	190.79	15.89	−3.28	51.5	−25.95	(−32.52; −18.67)	−20.92
CD13	246.95	18.42	−2.91	55.8	−22.43	(−28.43; −16.46)	−21.76
CD 14	260.27	18.58	−2.39	55.7	−21.85	(−26.23; −17.09)	−21.66
CD 15	197.37	16.19	−2.4	58.4	−22.32	(−27.17; −15.83)	−21.21
CD 16	212.55	16.82	−2.23	59	−23.15	(−28.12; −18.35)	−21.70
CD 19	224.84	17.47	−2.3	72.5	−27.15	(−34.41; −21.50)	−25.63
CD 20	392.31	25.44	−3.09	70.5	−28.12	(−36.30; −22.45)	−28.41

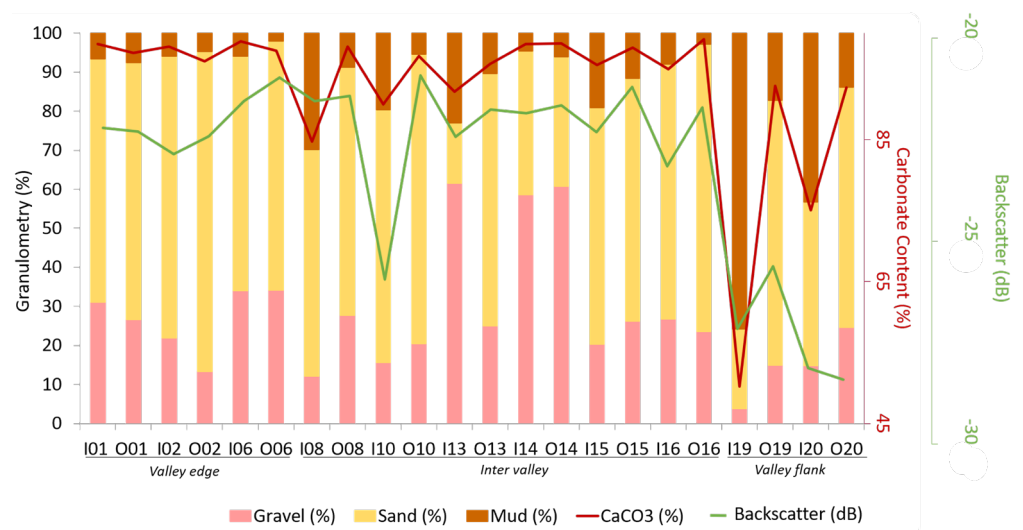


**Figure 7.** Grain size, carbonate content, and backscatter value for each sampled CD. “I” represents samples taken inside the depressions, and “O” represents samples outside.

#### 3.2.1. Circular Depressions on the Valley Edges

CDs in valley edges occur at water depths ranging from 55 to 63 m (Table 2) and are located on inclined terrain (Figure 5b',b''). Slightly coarser grain size content/higher backscatter intensity is present inside (Figure 7). Rhodoliths, carbonate fragments, and soft macroalgae are abundant and accumulate inside, while they are sparser outside (Figure 8). In terms of content, sediment samples are classified as carbonate sediments (>70% CaCO<sub>3</sub>) (Figure 7). No mounds or accumulation of coarse material were found on the edges. Fish burrows and bioturbation were observed, riddling the seabed with holes (Table 3). In addition, macrofauna we observed to be associated with CDs (Table 3).

**Table 3.** Depression images on valley edges.

CD 01 Inner	Outer
 <p>Aggregation of reddish rhodoliths and algae</p>	 <p>Spaced reddish rhodoliths</p>
CD 02 Inner	Outer
 <p>Aggregation of rhodoliths</p>	 <p>Spaced reddish rhodoliths</p>
CD 06 Inner	Outer
 <p>Aggregation of calcareous fragments</p>	 <p>Reddish rhodoliths and red algae</p>

3.2.2. Circular Depressions on Inter-Valley

CDs in the inter-valley region occur at a water depth ranging from 51 to 59 m (Table 2, Figure 5A,B). All sediment samples are classified as carbonate sediments (>80% CaCO<sub>3</sub>) (Figure 7). The backscatter intensity, despite exhibiting averages comparable to those observed in the valley edge samples, displayed a higher difference between the minimum and maximum values recorded within the features (Table 2; Figure 7). This difference was likely driven by the lower minimum values, which may be potentially associated with the presence of algae observed in the images (Table 4). Aggregations of calcareous algae with small fishes and other small-size biota were observed inside the CDs (CDs 8 and 10—Table 2). At the outer edge of the CDs, a positive relief was observed, formed by sand and carbonate gravel, including rhodoliths (Table 4). The material forming the mounds seems to have been extracted from inside the CD. Macroalgae diversity was noticed on these CDs, being more concentrated inside and sparser outside and usually associated with either rhodoliths or the crests of bedforms (Table 4). Fish burrows and bioturbation were visible, as an associated benthic macrofauna was observed (Table 4).

**Table 4.** Depression images on inter-valley.

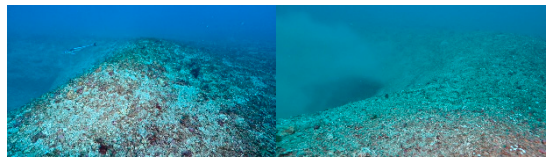
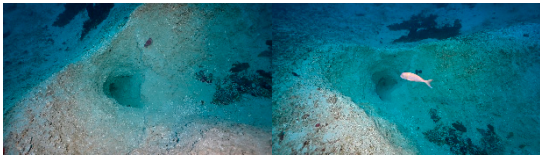
CD 08 Inner	Outer
 <p>Aggregation of whitish algae fragments</p>	 <p>Calcareous gravel and algae mound</p>

Table 4. Cont.

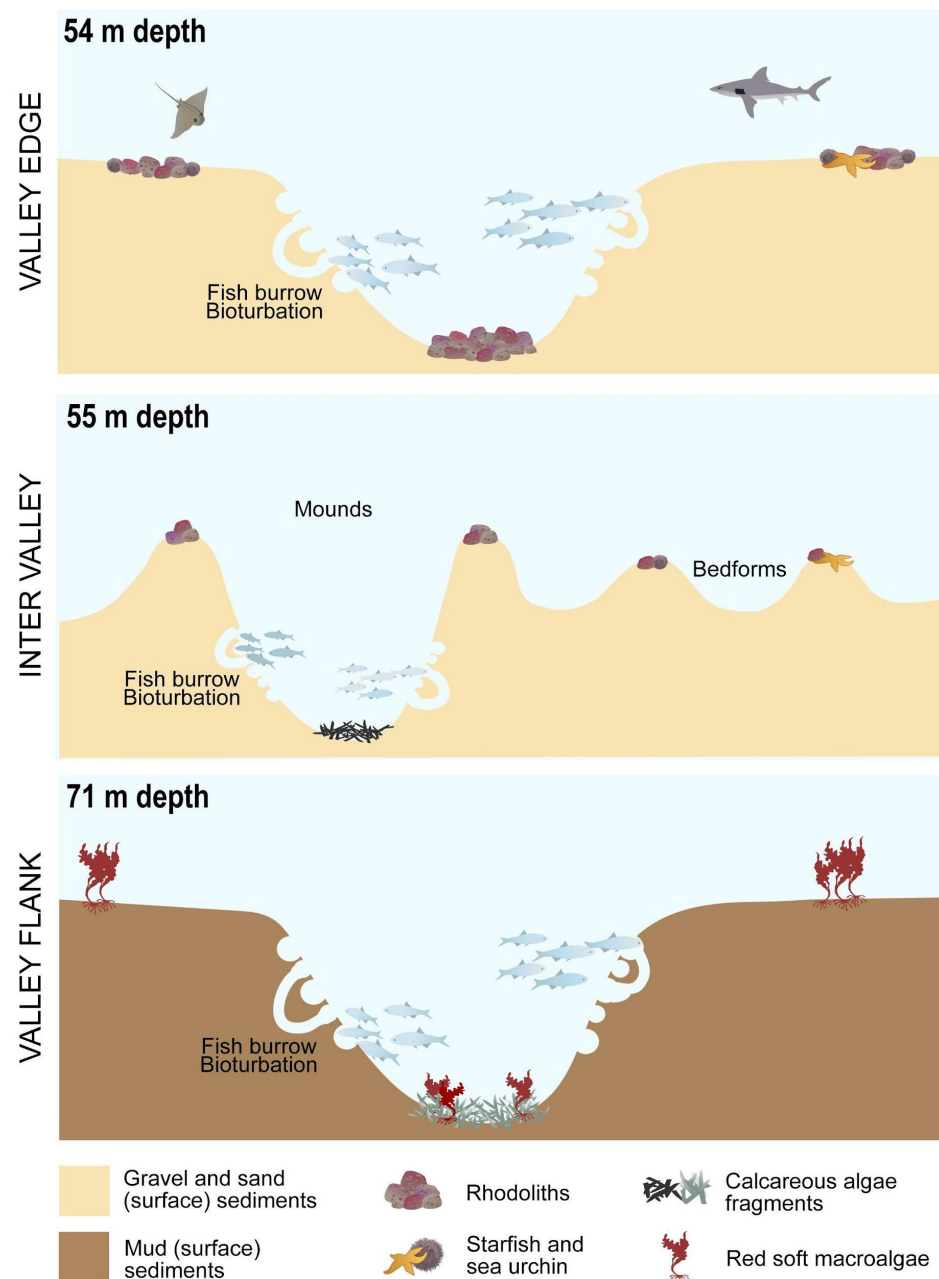
CD 10 Inner	Outer
	
Steepest “hole” with finer sediment	Spaced fragment and algae
CD 13 Inner	Outer
	
Aggregation of gravel and algae	Algae and gravel mounds
CD 14 Inner	Outer
	
Aggregation of gravel and algae	Spaced gravel and mounds
CD 15 Inner	Outer
	
Aggregations of algae and the presence of fish	Algae and gravel
CD 16 Inner	Outer
	
Aggregations of algae and the presence of fish	Algae and gravel mounds

### 3.2.3. Circular Depressions on Valley Flanks

CDs on the valley flanks are larger and deeper and occupy deeper water depths (Table 2). The sediment samples taken from the CDs in this morphological class are the only classified as mixed sediments (Figure 7). Sedimentological analysis revealed that on both CDs, on the inside, the mud fraction is abundant, while outside, there is more gravel fraction and carbonate content (Figure 7). Moreover, backscatter intensity exhibited the greatest divergence from the other sites; both the average and minimum backscatter levels were the lowest recorded, which is consistent with the finer sediment matrix imagery, as well as the higher mud contents (Table 2, Figure 7). Inside the CD, there is an agglomeration of calcareous algae associated with a diverse small-size biota (Table 5). The depression walls were noted to be sustained by a fine sediment matrix with a great number of bioturbation holes (Table 5). In addition, larger fish burrows were observed in these CDs (Table 5). The

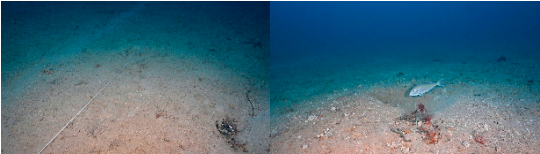
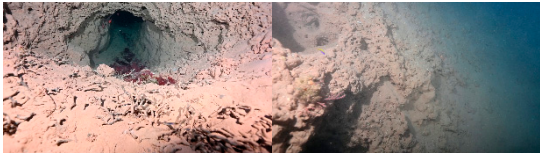
outer parts are flat without mounds, with some sparse concentration of algae associated with rhodoliths (Table 5).

Figure 8 is a schematic model constructed to summarize the mapped CDs. Usually, the deeper central parts of the circular depression appear to function as a sink, presenting aggregations of rhodoliths or coarser material. No changes were observed in the sediment composition inside and outside the depressions. In most inter-valley depressions, mounds are formed along the edges of the depression. Additionally, bedforms accumulating coarser material on the crest are found. Only non-carbonate samples were found on the valley flanks.



**Figure 8.** Schematic model of the circular depressions mapped in the area depicting a summary of the 3 categories: valley edge, inter-valley, and valley flanks. The depths shown on the model correspond to the mean water depth of the mapped depressions. Biota illustrated were spotted in the designated depressions. Gravel and sand correspond to carbonate content, while mud has mixed content (carbonate and terrigenous), according to [35].

**Table 5.** Depression images on the valley flanks.

CD 19 Inner	Outer
	
Aggregation of algae with a fine matrix and bioturbation indication	Spaced algae and fragments
CD 20 Inner	Outer
	
Aggregation of algae with a fine matrix and bioturbation indication	Spaced algae and fragments

## 4. Discussion

### 4.1. CD Acoustic Mapping and Characteristics

In the current study, 3660 CDs were identified, distributed in a morphologically heterogeneous seascape dominated by shelf-incised valleys. Although we have not quantitatively measured the accuracy of the delineations, the results are considered satisfactory by careful visual inspection, and intensive ground truthing is not required as the CDs are recognizably different from other shelf morphologies (similar logic to recognize pockmarks or reef features [34,36,37]). Moreover, as seen in the literature (e.g., [38]), the semi-automated approach has proven effective at reducing analysis time when compared to manual mapping. However, the occurrence of motion artifacts can pose challenges to the semi-automated process, potentially contributing to inaccuracies in the end product. The inclusion of a step involving the removal of polygons smaller than 50 m<sup>2</sup> and larger than 1000 m<sup>2</sup> was effective in preventing artifacts from being mistaken for real seafloor features. Nevertheless, we stress that the automatic delineation and, especially, the morphological characterization require an adequate match between the size of the real features, data quality, and the data resolution. Therefore, CDs in the Reason grid were manually mapped. Although no specific pattern was observed in the backscatter mosaic that could facilitate the identification of these features and was not a pivotal component in the automated identification of the CDs, it certainly contributed to a better understanding of the complex geodiversity. It could be further explored in future analyses (e.g., analysis of angular response curves). It is relevant to emphasize that the comparison was carried out between uncalibrated backscatter values in samples where ground truth was established utilizing data from the R2 Sonic system, which served as the reference for the bulk shift script. These comparisons were made on a relative basis, thereby avoiding any inconsistencies that might otherwise have arisen due to the use of different systems and excluding the possible effects due to the lack of acoustic calibration on the absolute values of backscatter.

### 4.2. Potential Origin of the CDs and Morphological Interpretation

The high-resolution bathymetry reveals that denser CD patches are found where the seafloor is complex and highly irregular, such as in valley edges and flanks or in the surroundings of positive features. This could indicate that valley-related processes could be either a trigger for their origin/formation or a mechanism for their current maintenance. CDs occupied an extensive unconsolidated seabed area dominated by rhodoliths and

carbonate fragments (Figure 9) [16,25]. The mapped area is a paleo-coastal and fluvial submerged landscape formed at low sea level when the continental shelf was subaerially exposed [39], allowing fluvial incision valleys to be formed across the continental shelves [20]. The predominance of extensive rhodolith beds and paleobarrriers along the continental shelf reflects the rapid rise in sea levels in tropical environments marked by the post-LGM transgression [20,40]. This abrupt alteration in the base level is also related to the development of the CDs. In addition, the study area is characterized by low sediment input and soft cliffs with associated narrow beaches and abrasion terraces; therefore, recent sedimentation is characterized by local biogenic production [41] and would explain why the CDs remain unburied and exposed.

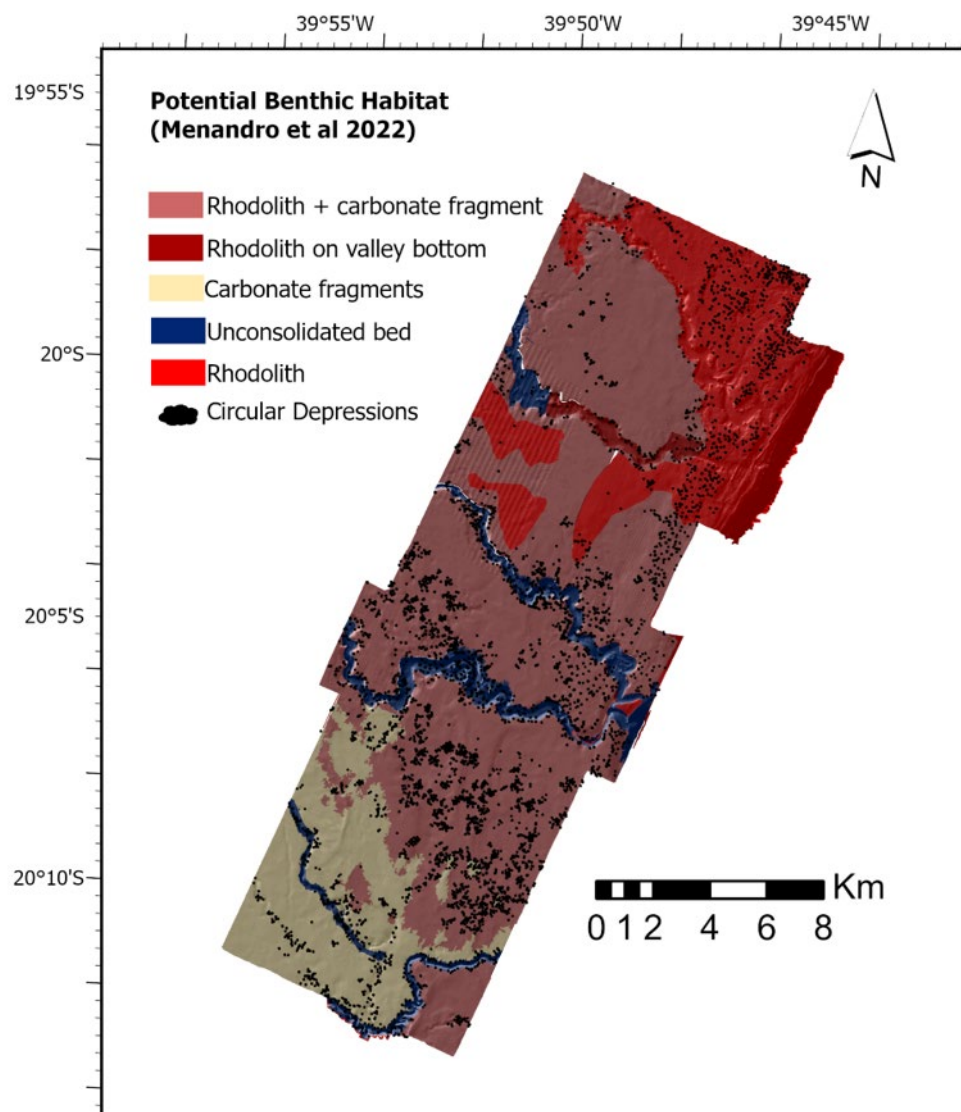


**Figure 9.** Potential benthic habitat map [23] overlapping hillshade bathymetry and circular depressions.

Similar seabed circular or non-circular depressions have been mapped and described throughout continental margins worldwide at several spatial scales at various water depths (Table 6). These depressions are usually described based on their formation processes; the most recurrent ones in tropical regions are pockmarks or sinkholes. Pockmarks are formed by fluid escape, which moves the unconsolidated fine sediment near the seafloor away, forming crater-like depressions [26], and sinkholes originate from carbonate dissolution during low-stand [42]. Even though the CDs observed in this study are not comparable with

many of these features in terms of diameter and relief, they exhibit similar characteristics, such as depth of occurrence and evidence of bioturbation (Table 6).

In Brazil, pockmarks were identified in deeper waters (300–700 m) with 1 km of diameter and relief of 100 m [43–48] associated with seepage of hydrocarbons from the seafloor close to oil exploration fields. This study did not find evidence of gas seepage in the area; however, a study [49] using Synthetic Aperture Radar imagery from the Radarsat-2 and Sentinel-1 identified 4 possible oil seeps within the Costa das Algas MPA.

**Table 6.** Worldwide distribution and characterization of circular depression-like features.

Feature Name	Location	Diameter (m)	Relief (m)	Depth (m)	Origin	Reference
Circular depressions	Costa das Algas MPA, Brazil	12.93 ( $\pm 4.1$ )	0.83 ( $\pm 0.7$ )	46–85	Unknown	This paper
Burrows	Hudson Submarine Canyon, USA	<5	2–3	110–230	Tilefish burrow construction associated with crabs	[28]
Pockmarks	North West Continental Shelf, Australia	5	1	45	Fish excavation	[29]
Pits	North Sea, Germany	19.4	0.05–0.2	28–28.5	Macrofauna burrow	[12]
Buracas	Abrolhos Bank, Brazil	10–75	8–39	24–65	Karstification	[27]
Pockmarks	North Sea, England	20–100	3–4	120–150	Gas escape	[23]
Pockmarks	Canterbury Margin, New Zealand	20	<1	80–140	Fluid flow and seepage	[30]
Pockmarks	Canterbury Margin, New Zealand	50–200	<20	500–1100	Fluid flow and seepage	[30]
Pockmarks	Brazil	1000	100	300–700	Hydrocarbon seepage in oil exploration fields	[44–48]
Pockmarks	Belfast Bay, Maine, USA	5		2.72–87.46	Methane escape linked to organic matter estuarine deposits	[37]
	Blue Hill Bay, Maine, USA	2	-	5.97–108.3		
	Passamoquoddy Bay, Maine, USA	1		0–88.15		
Pockmarks	California, USA	156	5	500–1500	Sediment gravity flow	[31]

In the Abrolhos Continental Shelf (170 km northward), ref. [50] described sinkholes (locally known as “Buracas”) with 10–75 m in diameter and 8–39 m in relief. Post-LGM sea-level rise resulted in carbonate accretion on top of the antecedent topography. Thus, recent sedimentation on these structures is represented by granular carbonate sediments or biogenic incrustation on the wall [41]. The buracas would record the drowning of this shelf during the post-glacial transgression, thereby helping to understand the shelf paleoenvironmental evolution [27]. World-famous sinkholes are described mainly in the Caribbean and are also known as Blue Holes [51].

Although it is difficult to prove any hypotheses about the origin of these depressions through time (dissolution, groundwater discharge, or fluid escape), they might yet be part of modern biotic processes such as bioturbation. Our observations show that burrows

are present in many of the visited CDs (Tables 3–5), indicating that, at least, there is a common fish behavior in the MPA outer shelf. Fish burrows may range from less than a meter to 20 m in diameter and relief of up to 3 m [29] in a variety of seabed sediment types, including carbonate [52] or siliciclastic [28,29]. The authors proved that fishes are physically capable of shaping holes in the seabed to provide themselves shelter. In the vicinities of the Hudson Canyon, for example, juvenile and adult tilefishes were observed swimming into the burrows with a head/tail-enter/exit pattern, evidencing that the hole is a refuge from predators, not to ambush prey. Additionally, the range of pit sizes found by [28] suggested that it is a progress sequence of burrow construction by tilefishes (up to 5 m in diameter and 2–3 m relief). An extensive field of shallow depressions along the North Sea with different shapes was mapped and described by [12]. The authors pointed out that their origin and evolution are related to seafloor excavations made by harbor porpoises during benthic foraging. Moreover, they described the presence of mounds on pit rims, a few centimeters higher than the surrounding seabed (0.1–0.2 m), without a preferred orientation. The potential influence of megafauna-driven macro-bioturbation was pointed out to reshape the seafloor [53]. Another example of fish inducing seafloor features was observed and described on the Fernando de Noronha Island shelf [54]. The authors described rhodolith mounds built by the sand tilefish *Malacanthus plumieri* (Bloch, 1786) and advocated for the ecological importance of this fish in the distribution and repositioning of rhodoliths. Although this behavior has not been described elsewhere, this species is well distributed along the Brazilian coast [55], overlapping rhodolith bed distribution [56,57].

#### 4.3. CDs and Benthic Habitat Implications

The origin of these depressions might not be reconstructed solely with the current dataset, but it is interesting to note that these compose a complex series of nested depressions with inter-depression variation (from microscale, centimeters, as the bioturbation shown in the valley flanks samples, to macroscale, meters, as the designated mapped features) that are probably “sustained” by the biota/fish burrows. The CDs produce a 3D seafloor feature that, naturally, tends to aggregate different sorts of materials in its bottom and concentrate biomass. We did not carry out a scientifically sound fish census or quantify the biomass associated with the CDs. However, the video footage obtained during the dives showed the presence of fishes in different life cycles, especially juvenile fishes swimming close to the macroalgae (complex 3D structure). Several fish species can play a vital role in physically shaping the seafloor and altering the benthos, with fish burrow density reaching over 2500/km<sup>2</sup> [58].

In this way, we first hypothesize that the formation of CDs can be attributed to a combination of paleo-processes that occurred during the last glacial period, when the shelf was exposed subaerially (forming larger holes), and modern processes linked to biomass aggregation and fish bioturbation (forming smaller secondary holes and rubble mounds). Further investigation is required to explore the ecological significance and the role played by this CD habitat.

## 5. Conclusions

One might expect to encounter new features and patterns at high resolution when exploring and mapping the seafloor. This study successfully employed both manual and semi-automated methods with multibeam bathymetry data as the primary input to spatially identify a circular depression macrohabitat. Additionally, it incorporated ground truthing data, which, combined with the mapping results, constitutes an important piece of information that can be used in the Costa das Algas MPA, which has the potential to contribute to conservation strategies in the region.

This contribution revealed 3600 circular depressions on the seafloor with an area of larger than 500 m<sup>2</sup> and relief of a maximum of 4 m. Even though the new findings are distributed along the entire highly heterogeneous area, the features are more concentrated in irregular seafloor portions, such as valley edges and flanks, and on the surroundings of positive relief, such as paleo-coastal barriers. This could indicate that inter-valley processes could be either a cause for their formation (origin) or a means to preserve them (maintenance).

The origin hypothesis needs to be further investigated with more data; so far, we believe that it could be related to sea-level variation and shelf exposure processes. Whether the depressions are relict features is still an open question, but it is suggested that their modern maintenance occurs in a smaller-scale process linked to biotic excavation. Regardless of the validity of the origin and maintenance hypothesis in multiple scales, one of the findings suggests the role played by CDs on biomass aggregation inside the depressions and, in some of them, outside forming mounds. In conclusion, the mapped area is composed of complex nested depressions with inter-depression variation (from microscale, centimeters, to a metric macroscale) that probably formed during low sea levels and are now “sustained” by biotic excavation. The CDs comprise important features for conservation as a surrogate for biodiversity, as it might enhance productivity and aggregate biomass.

Further analysis using innovative approaches and new technologies could contribute to a better understanding of localized, small-scale features, such as autonomous underwater vehicles (AUVs) and remotely operated vehicles (ROVs) to acquire seafloor and water column acoustic and imagery to create highly accurate and full coverage photomosaics of the seafloor and check potential seeps in the water column. The acquisition of high-resolution seismic reflection data could also help, although we are investigating a feature that is no more than 4 m in height. In addition to acoustic datasets, core samples and porewater detection analysis would also support the comprehensive interpretation of eliminating gas seeps and freshwater discharge or not.

**Author Contributions:** Conceptualization, A.C.L., M.D.L. and A.C.B.; methodology, A.C.L., M.D.L. and A.C.B.; software, A.C.L. and M.D.L.; validation, A.C.L. and M.D.L.; formal analysis, A.C.L., M.D.L., T.F., P.S.M., F.V.V. and G.C.B.; investigation M.D.L. and G.C.B.; resources A.C.B.; data curation, A.C.B.; writing—original draft preparation, A.C.L., M.D.L., T.F., P.S.M., F.V.V. and G.C.B.; writing—review and editing, A.C.B.; visualization, A.C.L., M.D.L., T.F., P.S.M. and A.C.B.; supervision, A.C.B.; project administration, A.C.B.; funding acquisition, A.C.B. All authors have read and agreed to the published version of the manuscript.

**Funding:** This research was funded by Renova Foundation and FEST/UFES as part of the the Aquatic Biodiversity Monitoring Program—PMBA project, the Long-term Ecological Study Program (FAPES-CNPq-CAPES) Peld-Abrolhos and the PRONEX-GeoMar, (FAPES).

**Data Availability Statement:** The raw data supporting the conclusions of this article will be made available by the authors on request.

**Acknowledgments:** Seabed mapping campaigns were part of the Aquatic Biodiversity Monitoring Program—PMBA project (Renova, UFES-FEST), Long-term Ecological Study Program (FAPES-CNPq-CAPES) Peld-Abrolhos, and the PRONEX-GeoMar project (FAPES). The authors thank Rodrigo Mello for acquiring the underwater images and sediment samples. We are also thankful to Joana Gafeira for the discussions on the automated mapping of the CD. This manuscript is a contribution to Rede Abrolhos.

**Conflicts of Interest:** The authors declare no conflicts of interest.

## References

1. Menandro, P.; Bastos, A. Seabed Mapping: A Brief History from Meaningful Words. *Geosciences* **2020**, *10*, 273. [[CrossRef](#)]
2. Robert, K.; Huvenne, V.A.I.; Georgiopoulou, A.; Jones, D.O.B.; Marsh, L.; Carter, G.D.O.; Chaumillon, L. New Approaches to High-Resolution Mapping of Marine Vertical Structures. *Sci. Rep.* **2017**, *7*, 9005. [[CrossRef](#)] [[PubMed](#)]
3. Misiuk, B.; Lecours, V.; Bell, T. A Multiscale Approach to Mapping Seabed Sediments. *PLoS ONE* **2018**, *13*, e0193647. [[CrossRef](#)] [[PubMed](#)]
4. Misiuk, B.; Lecours, V.; Dolan, M.F.J.; Robert, K. Evaluating the Suitability of Multi-Scale Terrain Attribute Calculation Approaches for Seabed Mapping Applications. *Mar. Geod.* **2021**, *44*, 327–385. [[CrossRef](#)]
5. Greene, H.G.; Bizzarro, J.J.; O’Connell, V.M.; Brylinsky, C.K. Construction of Digital Potential Marine Benthic Habitat Maps Using a Coded Classification Scheme and Its Application. *Geol. Assoc. Can. Spec. Pap.* **2007**, *47*, 141–155.
6. Lavagnino, A.C.; Bastos, A.C.; Amado Filho, G.M.; De Moraes, F.C.; Araujo, L.S.; De Moura, R.L. Geomorphometric Seabed Classification and Potential Megahabitat Distribution in the Amazon Continental Margin. *Front. Mar. Sci.* **2020**, *7*, 190. [[CrossRef](#)]
7. Dolan, M.; Bøe, R.; Bjarnadóttir, L.R. Delivering Seabed Geodiversity Information through Multidisciplinary Mapping Initiatives: Experiences from Norway. *GEUS Bull.* **2022**, *52*, 8325. [[CrossRef](#)]
8. Montereale-Gavazzi, G.; Roche, M.; Lurton, X.; Degrendele, K.; Terseleer, N.; Van Lancker, V. Seafloor Change Detection Using Multibeam Echosounder Backscatter: Case Study on the Belgian Part of the North Sea. *Mar. Geophys. Res.* **2018**, *39*, 229–247. [[CrossRef](#)]
9. Schimel, A.C.G.; Brown, C.J.; Ierodiaconou, D. Automated Filtering of Multibeam Water-Column Data to Detect Relative Abundance of Giant Kelp (*Macrocystis Pyrifera*). *Remote Sens.* **2020**, *12*, 1371. [[CrossRef](#)]
10. Lamarche, G.; Lurton, X.; Verdier, A.-L.; Augustin, J.-M. Quantitative Characterisation of Seafloor Substrate and Bedforms Using Advanced Processing of Multibeam Backscatter—Application to Cook Strait, New Zealand. *Cont. Shelf Res.* **2011**, *31*, S93–S109. [[CrossRef](#)]
11. Montereale Gavazzi, G.; Madricardo, F.; Janowski, L.; Kruss, A.; Blondel, P.; Sigovini, M.; Foglini, F. Evaluation of Seabed Mapping Methods for Fine-Scale Classification of Extremely Shallow Benthic Habitats—Application to the Venice Lagoon, Italy. *Estuar. Coast. Shelf Sci.* **2016**, *170*, 45–60. [[CrossRef](#)]
12. von Deimling, S.J.; Hoffmann, J.; Geersen, J.; Koschinski, S.; Lohrberg, A.; Gilles, A.; Belkin, I.; Böttner, C.; Papenmeier, S.; Krastel, S. Millions of Seafloor Pits, Not Pockmarks, Induced by Vertebrates in the North Sea. *Commun. Earth Environ.* **2023**, *4*, 478. [[CrossRef](#)]
13. Quaresma, V.S.; Bastos, A.C.; Leite, M.D.; Costa, A.; Cagnin, R.C.; Grilo, C.F.; Zogheib, L.F.; Santos Oliveira, K.S. The Effects of a Tailing Dam Failure on the Sedimentation of the Eastern Brazilian Inner Shelf. *Cont. Shelf Res.* **2020**, *205*, 104172. [[CrossRef](#)]
14. Franco, T.; Zorzal-Almeida, S.; Sá, F.; Bianchini, A.; Dergam, J.A.; Eskinazi-Sant’anna, E.M.; Albino, J.; Vieira, L.S.; Santos, L.G.M.; Ribeiro, A.P.L.; et al. *Ex-Post*. Impact Assessment on a Large Environmental Disaster. *Environ. Chall.* **2024**, *15*, 100889. [[CrossRef](#)]
15. Vieira, F.V.; Bastos, A.C.; Quaresma, V.S.; Leite, M.D.; Costa, A.; Oliveira, K.S.S.; Dalvi, C.F.; Bahia, R.G.; Holz, V.L.; Moura, R.L.; et al. Along-Shelf Changes in Mixed Carbonate-Siliciclastic Sedimentation Patterns. *Cont. Shelf Res.* **2019**, *187*, 103964. [[CrossRef](#)]
16. Oliveira, N.D.; Lavagnino, A.C.; Rocha, G.A.; Moura, R.L.D.; Bastos, A.C. Geomorphological Significance of Shelf-Incised Valleys as Mesophotic Habitats. *Front. Remote Sens.* **2023**, *4*, 1111825. [[CrossRef](#)]
17. Oliveira, N.; Bastos, A.C.; da Silva Quaresma, V.; Vieira, F.V. The Use of Benthic Terrain Modeler (BTM) in the Characterization of Continental Shelf Habitats. *Geo-Mar. Lett.* **2020**, *40*, 1087–1097. [[CrossRef](#)]
18. Bourguignon, S.N.; Bastos, A.C.; Quaresma, V.S.; Vieira, F.V.; Pinheiro, H.; Amado-Filho, G.M.; De Moura, R.L.; Teixeira, J.B. Seabed Morphology and Sedimentary Regimes Defining Fishing Grounds along the Eastern Brazilian Shelf. *Geosciences* **2018**, *8*, 91. [[CrossRef](#)]
19. Bastos, A.C.; D’Agostini, D.P.; Silva, A.E.; Menandro, P.S.; Vieira, F.V.; Boni, G.C.; Quaresma, V.S.; Cetto, P.H. Sedimentological and Morphological Evidences of Meltwater Pulse 1B in the Southwestern Atlantic Margin. *Mar. Geol.* **2022**, *450*, 106850. [[CrossRef](#)]
20. Ximenes Neto, A.R.; Quaresma, V.S.; Menandro, P.S.; Cetto, P.H.; Bastos, A.C. Drowned barriers and valleys: A morphological archive of base level changes in the western South Atlantic. *Mar. Geol.* **2024**, *477*, 107404. [[CrossRef](#)]
21. Rocha, G.A.; Bastos, A.C.; Amado-Filho, G.M.; Boni, G.C.; Moura, R.L.; Oliveira, N. Heterogeneity of Rhodolith Beds Expressed in Backscatter Data. *Mar. Geol.* **2020**, *423*, 106136. [[CrossRef](#)]
22. Menandro, P.S.; Misiuk, B.; Brown, C.J.; Bastos, A.C. Multispectral Multibeam Backscatter Response of Heterogeneous Rhodolith Beds. *Sci. Rep.* **2023**, *13*, 20220. [[CrossRef](#)] [[PubMed](#)]
23. Menandro, P.S.; Lavagnino, A.C.; Vieira, F.V.; Boni, G.C.; Franco, T.; Bastos, A.C. The Role of Benthic Habitat Mapping for Science and Managers: A Multi-Design Approach in the Southeast Brazilian Shelf after a Major Man-Induced Disaster. *Front. Mar. Sci.* **2022**, *9*, 1004083. [[CrossRef](#)]
24. Vieira, F.V.; Bastos, A.C.; Quaresma, V.S. Submerged Reef and Inter-Reef Morphology in the Western South Atlantic, Abrolhos Shelf (Brazil). *Geomorphology* **2023**, *442*, 108917. [[CrossRef](#)]

25. Menandro, P.S.; Bastos, A.C.; Misiuk, B.; Brown, C.J. Applying a Multi-Method Framework to Analyze the Multispectral Acoustic Response of the Seafloor. *Front. Remote Sens.* **2022**, *3*, 860282. [[CrossRef](#)]
26. King, L.H.; MacLean, B. Pockmarks on the Scotian Shelf. *GSA Bull.* **1970**, *81*, 3141–3148. [[CrossRef](#)]
27. Bastos, A.C.; Amado-Filho, G.M.; Moura, R.L.; Sampaio, F.M.; Bassi, D.; Braga, J.C. Origin and Sedimentary Evolution of Sinkholes (Buracas) in the Abrolhos Continental Shelf, Brazil. *Palaeogeogr. Palaeoclimatol. Palaeoecol.* **2016**, *462*, 101–111. [[CrossRef](#)]
28. Able, K.W.; Grimes, B.; Cooper, R.A.; Uzmann, J.R. Burrow Construction and Behavior of Tilefish, *Lopholatilus chamaeleonticeps*, in Hudson Submarine Canyon. *Environ. Biol. Fishes* **1982**, *7*, 199–205. [[CrossRef](#)]
29. Mueller, R.J. Evidence for the Biotic Origin of Seabed Pockmarks on the Australian Continental Shelf. *Mar. Pet. Geol.* **2015**, *64*, 276–293. [[CrossRef](#)]
30. Micallef, A.; Averages, T.; Hoffmann, J.; Crutchley, G.; Mountjoy, J.J.; Person, M.; Cohen, D.; Woelz, S.; Bury, S.J.; Ahaneku, C.V.; et al. Multiple Drivers and Controls of Pockmark Formation across the Canterbury Margin, New Zealand. *Basin Res.* **2022**, *34*, 1374–1399. [[CrossRef](#)]
31. Lundsten, E.; Paull, C.K.; Gwiadzda, R.; Dobbs, S.; Caress, D.W.; Kuhn, L.A.; Walton, M.; Nleminski, N.; McGann, M.; Lorensen, T.; et al. Pockmarks offshore Big Sur, California provide evidence for recurrent, regional, and unconfined sediment gravity flows. *J. Geophys. Res. Earth Surf.* **2024**, *129*, e2023JF007374. [[CrossRef](#)]
32. Misiuk, B.; Brown, C.J.; Robert, K.; Lacharité, M. Harmonizing Multi-Source Sonar Backscatter Datasets for Seabed Mapping Using Bulk Shift Approaches. *Remote Sens.* **2020**, *12*, 601. [[CrossRef](#)]
33. Gafeira, J.; Long, D.; Diaz-Doce, D. Semi-automated Characterisation of Seabed Pockmarks in the Central North Sea. *Near Surf. Geophys.* **2012**, *10*, 301–312. [[CrossRef](#)]
34. Gafeira, J.; Dolan, M.; Monteys, X. Geomorphometric Characterization of Pockmarks by Using a GIS-Based Semi-Automated Toolbox. *Geosciences* **2018**, *8*, 154. [[CrossRef](#)]
35. Larsonneur, C. La Cartographie Des Depots Meubles Sur Le Plateau Continental Français: Méthode Mise Au Point et Utilisée En Manche. *J. Recherché Océanographique* **1977**, *2*, 33–39.
36. Menandro, P.S.; Bastos, A.C.; Boni, G.; Ferreira, L.C.; Vieira, F.V.; Lavagnino, A.C.; Moura, R.L.; Diesing, M. Reef Mapping Using Different Seabed Automatic Classification Tools. *Geosciences* **2020**, *10*, 72. [[CrossRef](#)]
37. Lundine, M.A.; Brothers, L.B.; Trembanis, A.C. Deep learning for pockmark detection: Implications for quantitative seafloor characterization. *Geomorphology* **2023**, *421*, 108524. [[CrossRef](#)]
38. Lioupa, V.; Karsiotis, P.; Arosio, R.; Hasiotis, T.; Wheeler, A.J. A Comparative Crash-Test of Manual and Semi-Automated Methods for Detecting Complex Submarine Morphologies. *Remote Sens.* **2024**, *16*, 4093. [[CrossRef](#)]
39. Lambeck, K.; Rouby, H.; Purcell, A.; Sun, Y.; Sambridge, M. Sea Level and Global Ice Volumes from the Last Glacial Maximum to the Holocene. *Proc. Natl. Acad. Sci. USA* **2014**, *111*, 15296–15303. [[CrossRef](#)]
40. Nalin, R.; Nelson, C.S.; Basso, D.; Massari, F. Rhodolith-bearing Limestones as Transgressive Marker Beds: Fossil and Modern Examples from North Island, New Zealand. *Sedimentology* **2008**, *55*, 249–274. [[CrossRef](#)]
41. Bastos, A.C.; Quaresma, V.S.; Marangoni, M.B.; D’Agostini, D.P.; Bourguignon, S.N.; Cetto, P.H.; Silva, A.E.; Amado Filho, G.M.; Moura, R.L.; Collins, M. Shelf Morphology as an Indicator of Sedimentary Regimes: A Synthesis from a Mixed Siliciclastic–Carbonate Shelf on the Eastern Brazilian Margin. *J. S. Am. Earth Sci.* **2015**, *63*, 125–136. [[CrossRef](#)]
42. Díaz-Mendoza, G.A.; Krämer, K.; Von Rönn, G.A.; Schwarzer, K.; Heinrich, C.; Reimers, H.-C.; Winter, C. Circular Structures on the Seabed: Differentiating between Natural and Anthropogenic Origins—Examples from the Southwestern Baltic Sea. *Front. Earth Sci.* **2023**, *11*, 1170787. [[CrossRef](#)]
43. Land, L.A.; Paull, C.K.; Hobson, B. Genesis of a Submarine Sinkhole without Subaerial Exposure: Straits of Florida. *Geology* **1995**, *23*, 949–951. [[CrossRef](#)]
44. Sumida, P.Y.G.; Yoshinaga, M.Y.; Madureira, L.A.S.-P.; Hovland, M. Seabed Pockmarks Associated with Deepwater Corals off SE Brazilian Continental Slope, Santos Basin. *Mar. Geol.* **2004**, *207*, 159–167. [[CrossRef](#)]
45. Cooke, C.V.; Madureira, L.S.P.; Griep, G.H.; Pinho, M.P.D. Análise de Dados de Ecossondagem de Fundo Oriundos de Cruzeiros Realizados Entre Fortaleza (CE) e Chuí (RS) Com Enfoque Na Morfologia e Tipos de Fundo. *Rev. Bras. Geof.* **2007**, *25*, 443–457. [[CrossRef](#)]
46. Mueller, D.J.; Ketzer, J.M.; Viana, A.R.; Kowsmann, R.O.; Freire, A.F.M.; Oreiro, S.G.; Augustin, A.H.; Lourega, R.V.; Rodrigues, L.F.; Heemann, R.; et al. Natural Gas Hydrates in the Rio Grande Cone (Brazil): A New Province in the Western South Atlantic. *Mar. Pet. Geol.* **2015**, *67*, 187–196. [[CrossRef](#)]
47. Mahiques, M.M.; Schattner, U.; Lazar, M.; Sumida, P.Y.G.; Souza, L.A.P.D. An Extensive Pockmark Field on the Upper Atlantic Margin of Southeast Brazil: Spatial Analysis and Its Relationship with Salt Diapirism. *Heliyon* **2017**, *3*, e00257. [[CrossRef](#)]
48. Ramos, R.B.; Dos Santos, R.F.; Schattner, U.; Figueira, R.C.L.; Bicego, M.C.; Lobo, F.J.; De Mahiques, M.M. Deep Pockmarks as Natural Sediment Traps: A Case Study from Southern Santos Basin (SW Atlantic Upper Slope). *Geo-Mar. Lett.* **2020**, *40*, 989–999. [[CrossRef](#)]

49. Correa do Espirito Santo, L.D.A.; dos Santos Salomão, M.; Campos Pedroso, E.; Appi, C.J. Oil Seep Detection Using Microwave Remote Sensing at Espírito Santo Basin, Eastern Brazil. *Anuário Inst. Geociências* **2023**, *46*, 48346. [[CrossRef](#)]
50. Bastos, A.C.; Moura, R.L.; Amado-Filho, G.M.; D'Agostini, D.P.; Secchin, N.A.; Francini-Filho, R.B.; Güth, A.Z.; Sumida, P.Y.G.; Mahiques, M.M.; Thompson, F.L. Buracas: Novel and Unusual Sinkhole-like Features in the Abrolhos Bank. *Cont. Shelf Res.* **2013**, *70*, 118–125. [[CrossRef](#)]
51. Mylroie, J.E.; Carew, J.L.; Moore, A.I. Blue Holes: Definition and Genesis. *Carbonates Evaporites* **1995**, *10*, 225–233. [[CrossRef](#)]
52. Stieglitz, T. Habitat Engineering by Decadal-Scale Bioturbation around Shipwrecks on the Great Barrier Reef Mid-Shelf. *Mar. Ecol. Prog. Ser.* **2013**, *477*, 29–40. [[CrossRef](#)]
53. Vallim, A.; Schenone, S.; Thrush, S. Megafauna: The Ignored Bioturbators. *Mar. Ecol. Prog. Ser.* **2024**, *733*, 137–144. [[CrossRef](#)]
54. Amado-Filho, G.M.; Pereira-Filho, G.H.; Bahia, R.G.; Abrantes, D.P.; Veras, P.C.; Matheus, Z. Occurrence and Distribution of Rhodolith Beds on the Fernando de Noronha Archipelago of Brazil. *Aquat. Bot.* **2012**, *101*, 41–45. [[CrossRef](#)]
55. Clark, E.; Pohle, J.F.; Halstead, B. Ecology and behavior of tilefishes, *Hoplolatilus starcki*, *H. fronticinctus* and related species (Malacanthidae): Non-mound and mound builders. *Environ. Biol. Fishes* **1998**, *52*, 395–417. [[CrossRef](#)]
56. Foster, M.S. Rhodoliths: Between Rocks and Soft Places. *J. Phycol.* **2001**, *37*, 659–667. [[CrossRef](#)]
57. Amado-Filho, G.M.; Maneveldt, G.W.; Pereira-Filho, G.H.; Manso, R.C.; Bahia, R.G.; Barros-Barreto, M.B.; Guimarães, S.M. Seaweed Diversity Associated with a Brazilian Tropical Rhodolith Bed. *Cienc. Mar.* **2010**, *36*, 371–391. [[CrossRef](#)]
58. Twichell, D.C.; Grimes, C.B.; Jones, R.S.; Able, K.W. The Role of Erosion by Fish in Shaping Topography Around Hudson Submarine Canyon. *SEPM J. Sediment. Res.* **1985**, *55*, 712–719. [[CrossRef](#)]

**Disclaimer/Publisher's Note:** The statements, opinions and data contained in all publications are solely those of the individual author(s) and contributor(s) and not of MDPI and/or the editor(s). MDPI and/or the editor(s) disclaim responsibility for any injury to people or property resulting from any ideas, methods, instructions or products referred to in the content.